

Engineering Impurity Distributions in Photoelectrodes for Solar Water Oxidation

Coleman X. Kronawitter,* Zhixun Ma, Dongfang Liu, Samuel S. Mao,*
and Bonnie R. Antoun

The distinction between electricity and fuel use in analyses of global power consumption statistics highlights the critical importance of establishing efficient synthesis techniques for solar fuels—those chemicals whose bond energies are obtained through conversion processes driven by solar energy.^[1] Photoelectrochemical (PEC) processes show potential for the production of solar fuels because of their demonstrated versatility in facilitating optoelectronic and chemical conversion processes.^[2] Tandem PEC-photovoltaic modular configurations for the generation of hydrogen from water and sunlight (solar water splitting) provide an opportunity to develop a low-cost and efficient energy conversion scheme.^[3,4] The critical component in devices of this type is the PEC photoelectrode, which must be optically absorptive, chemically stable, and possess the required electronic band alignment with the electrochemical scale for its charge carriers to have sufficient potential to drive the hydrogen and oxygen evolution reactions. After many decades of investigation, the primary technological obstacle remains the development of photoelectrode structures capable of efficient conversion of light with visible frequencies, which is abundant in the solar spectrum.^[5] Metal oxides represent one of the few material classes that can be made photoactive and remain stable to perform the required functions.^[6,7] This report presents a strategy to decouple the crucial optical absorption and electronic transport processes required for operation of metal oxide photoelectrodes by spatially segregating the functional impurity concentrations that facilitate their associated physical processes.

One technique to sensitize metal oxides to visible light is to introduce dopants that are associated with visible-light-active

electronic transitions.^[8,9] If dopant species are introduced in low concentration, below the substitutional limit in the host oxide lattice, optical spectroscopy measurements of films and particle suspensions (typical photoelectrode and photocatalyst configurations) commonly indicate weak shoulders associated with dopant-induced light absorption relative to the host's band-edge absorption.^[10] This observation relates to the comparably lower density of states of absorbing impurity levels within the host oxide band structure: because the solubilities of many dopants of interest are restricted to a few atomic percent,^[8] for nearly equivalent cross sections dopant-induced absorption is expected to be an inherently weaker process than absorption directly effected by the host oxide band structure. Heavily doping beyond the substitutional limit will assist further in sensitization, but with an associated sacrifice of crystallographic order in the surrounding lattice.

Consequently, in order to achieve optical thickness at these weakly absorbing wavelengths, the path length within the electrode structure must be increased, which for conventional film-based electrodes requires the fabrication of physically thick structures. The use of thick films, however, is problematic because of the generally poor transport of carriers in metal oxides, and especially carriers associated with isolated impurity states. The disparity between absorption lengths and transport lengths in oxide materials of interest for this application is addressed generally in the growing literature dedicated to the use of nanotechnologies for solar PEC hydrogen generation.^[7]

These observations suggest that doping traditional metal oxide photoelectrodes presents the unacceptable situation where many free carriers generated by visible light excitations recombine before reaching the rear contact or reacting electrochemically at the oxide-liquid interface. Consequently, a viable strategy to enhance the conversion efficiencies of doped metal oxide-based photoelectrodes should be to decouple the optical absorption and electronic conduction processes that occur during their operation. In order to accomplish this, the electrode architecture must be designed such that the associated physical phenomena are segregated, while maintaining spatial register among the facilitating structure regions.

Fortunately, the technological implementation of weakly absorptive materials with poor charge transport properties has been comprehensively addressed in the various designs for metal-oxide-containing excitonic photovoltaic devices.^[11] In these devices, organic dyes^[12] or semiconductor nanocrystals^[13] are intimately contacted with media whose operational purpose is to selectively accept (or separate) and transport photogenerated charges for collection in an external circuit. This configuration has also been applied toward the photoelectrochemical

C. X. Kronawitter, Dr. S. S. Mao
Department of Mechanical Engineering
University of California
Berkeley, Mail Code 1740, 6141 Etcheverry Hall
University of California
Berkeley, CA 94720-1740, USA
E-mail: coleman@me.berkeley.edu; ssmao@lbl.gov

C. X. Kronawitter, Dr. Z. Ma, Dr. D. Liu, Dr. S. S. Mao
Environmental Energy Technologies Division
Lawrence Berkeley National Laboratory
1 Cyclotron Road, Mail Stop 70-108B, USA
Berkeley, CA 94720, USA

Dr. B. R. Antoun
Sandia National Laboratories
P.O. Box 969, MS 9042, Livermore, CA 94551-0969, USA



DOI: 10.1002/aenm.201100425

generation of hydrogen in electrolytes containing sacrificial reagents to considerable success.^[14] If the concept is applied toward the fabrication of metal oxide photoelectrodes for water splitting an analogy can be drawn between the sensitizer phase and a doped, visible-light-active oxide crystal, in that both of these materials are optically absorptive in the spectral range of interest but efficiently transport charges only over short physical distances. Deposition onto nanostructured substrates permits the use of absorber layers with small physical thickness but large optical thickness (as realized for example in extremely-thin-absorber photovoltaic cells^[15] and α -Fe₂O₃ photoanodes^[16,17]). If the substrate is of the same character as the sensitizer phase, the conceptual outcome of this application is a single-phase, oxide nanostructure that is inhomogeneously doped to perform the optoelectronic conversion processes relevant to the oxidation of water using solar energy. The isostructural nature of the absorbing and conducting regions in this case has the potential to yield low concentrations of interface recombination centers, which has significant consequences on the overall conversion efficiencies of PEC devices.

The concept is presently demonstrated with ZnO nanostructures doped in core regions with shallow Al donor levels for enhanced electronic conduction and in the near-surface volume with intragap Ni impurity states for increased optical absorption. However, the strategy is quite general and can be applied to numerous oxides and impurities; additional experiments were conducted with photoactive nitrogen impurities in place of nickel, with similar, albeit less-pronounced, PEC performance enhancements evident. **Figure 1** provides electron microscopy images of the complete structures as well as a schematic of the proposed operating mechanisms within the oxide structure described later in this report; its composition is discussed in detail below. The change in morphology upon introduction of ZnO:Ni is shown in Figure S1.

Substitutional Al is a shallow donor in the ZnO nanocrystal lattice and is associated with large increases of electronic conductivity, which result from an order of magnitude increase in carrier concentration.^[18] The ionization energy of Al states has been measured to be approximately 90 meV.^[19] It is therefore identified as a suitable dopant to facilitate enhanced electronic conduction to the rear contact during PEC operation.

Visible light sensitization on the other hand involves the introduction of impurity states deeper within the bandgap of ZnO. Substitutional impurities on the cation site can be used to functionally sensitize ZnO crystals if they introduce impurity levels or bands that are situated at potentials meeting the thermodynamic requirement for water oxidation. The requirement is met by a number of transition metal impurities; the mechanism by which these impurities sensitize ZnO to visible wavelengths will be discussed later in this report.

An X-ray diffraction pattern (**Figure 2a**) after fabrication indicates the presence of hexagonal ZnO and the tetragonal SnO₂ substrate (FTO). The ZnO is highly (002)-textured, which results from the c-axis alignment of nanostructures normal to the substrate. The small unlabeled peaks around 26° and 56° were present in all ZnO samples regardless of dopant composition, and are tentatively attributed to a contamination artifact from the fabrication procedure.

The optical absorbance spectra of ZnO nanostructure arrays deposited onto FTO substrates with and without the introduction of crystallites doped with Ni are shown in **Figure 2b**. The absorption features beyond 400 nm are associated with a change in sample color from transparent-white to green (see sample photographs in **Figure 2c**), which is consistent with previous reports.^[20] A reference ZnO:Ni thin film, deposited under identical conditions directly onto the FTO substrate, is also included in **Figures 2b** and **Figures 2c**. Comparison of these optical properties highlights the dramatic increase in optical thickness at visible wavelengths that is associated with the nanostructured homojunction architecture.

The broad absorption features at long wavelengths overlap with transitions associated with tetrahedrally coordinated Ni(II) in the ZnO lattice. Examination of the diffuse reflectance spectra for ZnO:Al and ZnO:Al-ZnO:Ni on FTO/glass substrates in **Figure 2d** provides additional resolution for these transitions. The dashed lines in this figure indicate the known electronic transitions associated with Ni(II) with tetrahedral symmetry.^[20,21] The plot indicates reflectance features at these wavelengths that are introduced along with Ni-doped ZnO crystallites, which suggest a tetrahedral coordination of Ni(II).

Photoelectrochemical characterization of the ZnO/FTO electrodes in aqueous 0.5 M Na₂SO₄ provides confirmation of the

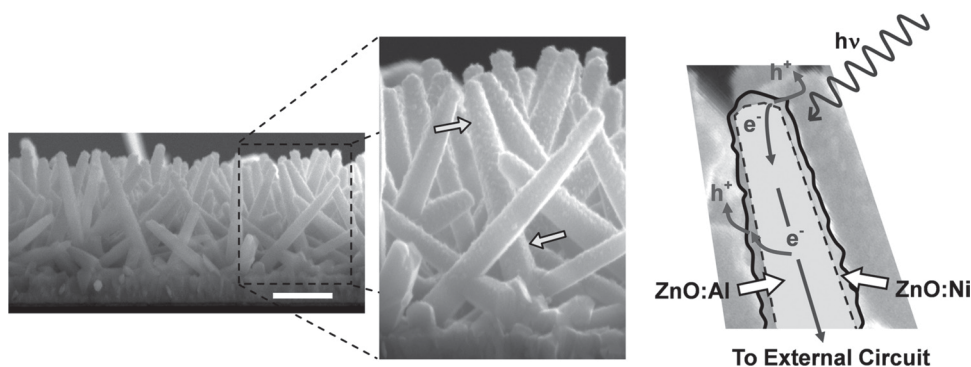


Figure 1. Scanning electron microscopy images of ZnO nanostructure arrays, with arrows highlighting doped crystallites distributed approximately 1.5 μm along the direction of light propagation. White scale bar indicates 1 μm . Right hand side provides a schematic of idealized operating mechanisms overlaid onto the tip of an individual nanostructure.

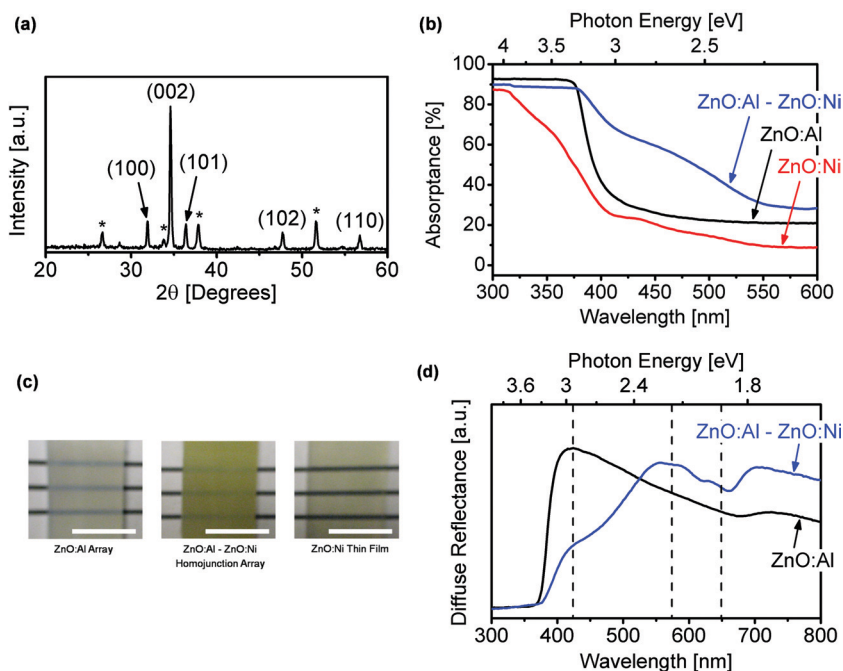


Figure 2. Structural and optical characterization of ZnO nanostructure arrays with and without ZnO:Ni modification: (a) X-ray diffraction pattern of final ZnO nanostructure array. Hexagonal ZnO (wurtzite) is indexed; tetragonal SnO₂ (cassiterite) substrate peaks indicated by □. (b) Absorbance spectra ($A_\lambda = 100 - T_\lambda - R_\lambda$) of ZnO/FTO/glass structures. (c) Photographs of ZnO:Al array (left), ZnO:Al-ZnO:Ni array (middle), and ZnO:Ni thin film (right). White scale bars indicate 1 cm. (d) Diffuse reflectance spectra; dashed lines indicate electronic transitions established in the literature for Ni(II) with tetrahedral symmetry in the ZnO lattice (see main text for details).

concept's successful application toward visible-light-driven solar water splitting. Current-potential curves (Figure 3a) indicate a monotonic photocurrent increase with applied anodic potential until the onset of dark current, which suggests effective charge separation at the semiconductor-liquid junction.^[22] Insertion of a UV filter in the optical path, which eliminates wavelengths below 410 nm, causes a moderate decrease in photocurrent response. The magnitude of the contribution of UV-driven photoactivity to total activity is explained by the comparably small UV photon flux available in solar (simulated) light (approximately 5% of intensity). Amperometric (current-time) measurements with application of color filters shown in Figure 3b indicate the portion of total photocurrent driven by visible light. In these conditions approximately 44% of total photocurrent originates from wavelengths beyond 410 nm; 4.4% originates from beyond 510 nm. Similar analyses of ZnO electrodes without Ni indicate the photocurrent is almost completely UV-driven (see Figure S5).

The incident photon conversion efficiency (IPCE) at visible wavelengths for front-side irradiation and with +1 V applied versus a Pt counter electrode is presented in Figure 3c. There is a marked decrease (ca. 4 times) of UV photoactivity upon addition of ZnO:Ni species (see Figure S4), which can be understood by observation that all photoholes originating from UV excitation must pass through impure visible-light-active crystals at the ZnO-water interface. Efficiency losses of this type can be minimized through the general optimization of electrode architecture, as discussed below.

To investigate the effect of the homojunction architecture on visible-light-driven water oxidation efficiency, the IPCE spectrum of a dense ZnO:Ni thin film deposited under identical conditions is compared to the nanostructured homojunction array. Presented in Figure 3c, these data indicate that approximately a three-fold enhancement in conversion efficiencies for solar-abundant visible wavelengths is achieved by distributing the absorptive species normal to the substrate and along the direction of light propagation. It is determined that the design effectively shifts the spectral photocurrent response of ZnO electrodes toward lower energies abundant in the solar spectrum.

D. Fichou *et al.* examined the spectral photocurrent contribution toward water oxidation of isovalent Mn²⁺, Co²⁺, and Ni²⁺ dopants in ZnO polycrystalline photoanodes.^[20] It was suggested that visible light photoactivity originated from *d-d* transitions within the dopant ion, with subsequent charge transfer into the ZnO band structure. In this interpretation, photoelectrons originating from impurity 3dⁿ excitations were transferred to the ZnO conduction band (Zn 4s⁰ orbitals); holes were transported to the ZnO-electrolyte interface in a defect band and were electrochemically active in a buffered Na₂SO₄ solution.

More recently however, work from D. R. Gamelin and coworkers^[23–26] has unambiguously determined that charge transfer states are required to generate observable photocurrents associated with transition metal dopants in ZnO. Based on these previous analyses of ZnO:Co^[24] and ZnO:Ni,^[23] excitations with wavelengths near 430 nm can be assigned to an acceptor-type ionization, where an electron is promoted to the dopant *d*-shell orbitals from ZnO-based donor orbitals of the valence band.^[24] If the ZnO lattice is considered a ligand of the dopant ion, these transitions fit the general description of ligand-to-metal charge transfer transitions. The excited state of the charge transfer transition in this case is a valence band hole Coulombically bound to a Ni⁺ dopant ion. This can be deduced from the numerous previous analyses of isovalent transition metal dopants in ZnO and other II–VI semiconductor lattices.^[23,24,26,27] References [23] and [27] suggest the excitation can be described as



The bound carrier generated from this excitation should possess a hydrogen-like wavefunction^[23] and a potentially large orbital radius,^[27] but one which is reduced relative to a free hole. In the context of this assignment, it is clear that the efficient utilization of valence band charge transfer transitions for solar water oxidation will require the use of thin doped regions that are located in close proximity to the electrolyte.

Based on these optical and photoelectrochemical data and the literature cited in this article, some conclusions can be drawn regarding the electronic band structures of the

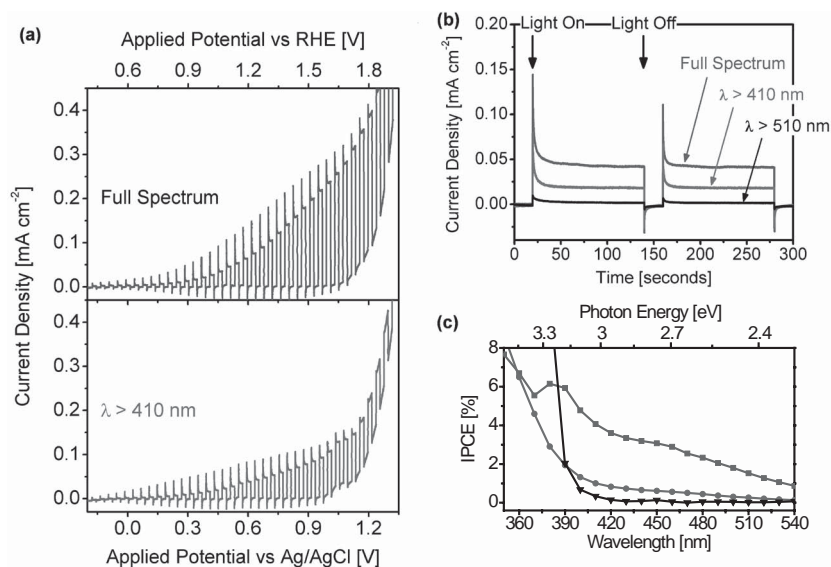


Figure 3. Photoelectrochemical characterization of ZnO electrodes in 0.5 M Na₂SO₄: (a) Current density-potential curve under chopped AM 1.5G-filtered 100 mW cm⁻² solar-simulated irradiation with and without application of a UV filter. (b) Amperometric (current-time) measurement at 0.6 V versus Ag/AgCl with chopped AM 1.5G-filtered 100 mW cm⁻² irradiation, with application of wavelength filters. (c) Incident photon conversion efficiency at visible wavelengths for ZnO:Al-ZnO:Ni homojunction array (blue squares), ZnO:Ni thin film (red circles), and ZnO:Al nanorod array (black triangles), with +1 V applied versus a Pt counter electrode.

inhomogeneously doped nanostructures. The carrier transfer under irradiation, confirmed by the above photoelectrochemical characterization, was depicted schematically in the right hand side of Figure 1. The band diagram in Figure 4 reflects the theoretical understanding of photoanode operation established in the literature^[28] but is augmented by the literature-derived electronic states matching the profiles in the structures.

In order to investigate the nature of the observed efficiency enhancements at visible wavelengths, the internal quantum efficiency, or absorbed photon conversion efficiency, of the samples

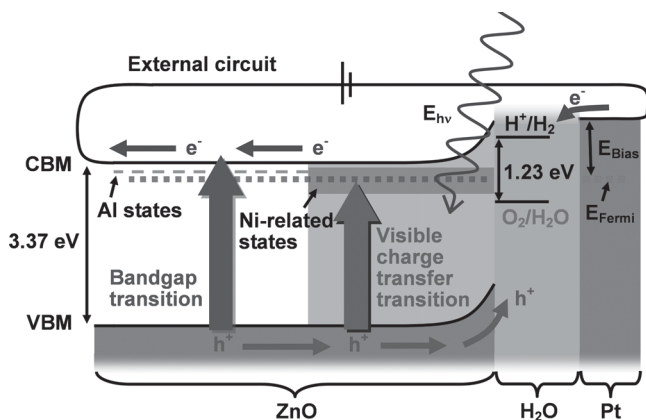


Figure 4. Idealized energetics of the functional homojunction nanostructures demonstrated in this study. Note that surface/interface and other defect states are likely to be present but are omitted in the diagram as they were not studied experimentally. Relative positions of electronic states are schematic but based on literature values (see main text).

were calculated. These efficiencies were calculated through the following equations:

$$T_{\text{measured}} = T_1 \times T_2 \times \dots \times T_n \quad (2)$$

$$T_{\lambda, \text{film}} = \frac{T_{\lambda, \text{measured}}}{T_{\lambda, \text{substrate}}} \quad (3)$$

$$A_{\lambda} = -\ln(T_{\lambda, \text{film}}) \quad (4)$$

$$\text{LHE}_{\lambda} = 1 - e^{-A_{\lambda}} \quad (5)$$

$$\text{APCE}_{\lambda} = \frac{\text{IPCE}_{\lambda}}{\text{LHE}_{\lambda}} \quad (6)$$

Where T_n is the transmittance of a component in the layered structure, $T_{\lambda, \text{film}}$ is the transmittance of the film, corrected for the substrate as from equation (2) and equation (3), A_{λ} is the absorbance, LHE_{λ} is the light harvesting efficiency, and APCE_{λ} is the absorbed photon conversion efficiency. The LHE and APCE as calculated from the above equations are plotted in Figure 5. The magnitudes of the APCE values increase dramatically for wavelengths where there is little light absorption, which results in oscillations in the curves corresponding to those in the LHE spectra.

These curves indicate that both the LHE and APCE at visible wavelengths are increased by distributing ZnO:Ni vertically along the direction of light propagation. The variation in the APCE values over this spectral range may indicate differences in intrinsic escape probabilities for photogenerated electrons and holes.^[24] Longer wavelength excitations may correspond to

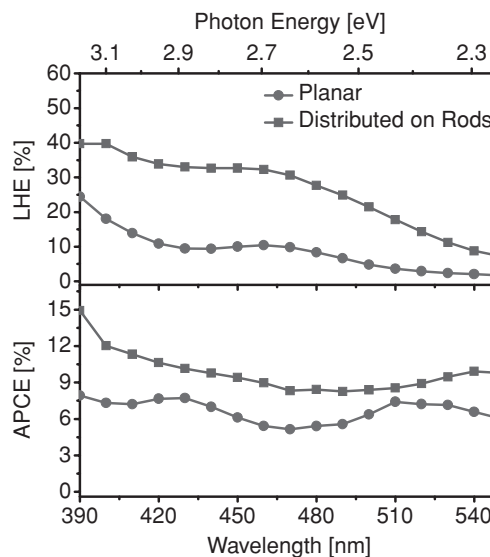


Figure 5. Light harvesting efficiency (top panel) and absorbed photon conversion efficiency (bottom panel) as defined in the main text. Blue squares correspond to efficiencies when ZnO:Ni is distributed on nanorods along the direction of light propagation; red circles correspond to those for a planar ZnO:Ni thin film.

alternative excitations, such as those related to metal-to-ligand charge transfer transitions, which have different branching ratios for charge separation in their excited states. The transitions could be sensitized by an optical absorption band near 2.9 eV, which would tend to flatten the *IPCE* curve relative to the *APCE* curve. In Figure 5, the oscillations in *APCE* are present in both planar and distributed configurations, which suggests they are related to the electronic structure of the material itself. More in-depth analyses of the material's electronic structure would be required to elucidate the nature of these transitions.

This observation of enhanced *LHE* and *APCE* provides confirmation of the proposed benefits of the homojunction architecture discussed above: greater *LHE* suggests an enhancement in optical absorption and greater *APCE* at visible wavelengths suggests an enhancement in charge separation. Because the thickness of the photoactive layer is reduced by distributing species over a larger surface area substrate, the design facilitates shorter carrier transport path lengths to phases where carrier extraction occurs. This result may also suggest that electrons excited from charge transfer transitions within the ZnO band-structure are more easily transferred to the ZnO:Al phase than to the SnO₂:F substrate.

In an optimized photoelectrode, the dopant profiles within the structures should be tailored to maximize conversion efficiency, which depends on, among other quantities, the free electron mobility and concentration, minority carrier (hole) transport length, and extinction coefficient. The metal oxide's feature dimensions should be constructed to maximize both the spectral overlap of optical absorption with the terrestrial solar flux and quantity of photogenerated minority carriers reaching the oxide-water interface.

As part of an initial effort toward design optimization, the optical functions of a ZnO:Ni thin film were approximated by a combined ellipsometry-reflectometry technique (see Supporting Information for details), the results of which are consistent with previous measurements of metal-doped ZnO films.^[29] These analyses accurately determine the complex refractive index and associated spectral absorption coefficient of the film. The light penetration depths determined by this spectral quantity (Figure S3) suggest that the optimal structure dimension in the direction of light propagation is on the order of several micrometers, which could be reduced by accounting for the significant light scattering effects associated with irradiation of nanowire arrays.^[30]

Here again a close analogy can be drawn to the design of dye-sensitized solar cells, which require dye molecule adsorption over several micrometers of porous structure to achieve optical thickness.^[12] Careful analyses of SEM images such as those in Figure 1 indicate the absorptive crystallites are distributed for as long as 1.5 μm along the direction of light penetration. The demonstrated efficiency enhancement in Figure 3c is conceptually similar to the dramatic enhancement evident in dye-sensitized solar cells when planar TiO₂ dye adsorption substrates are replaced with nanostructured TiO₂.^[31] It is suggested that an optimization route for fabrication of efficient homojunction nanostructures of this type is analogous to maximization of dye loading in dye-sensitized solar cells—optimization requires the select doping of the near-surface volume of porous nanostructures over several micrometers.

There is in fact an all (electro)chemical route to the fabrication of metal oxide homojunction nanostructure arrays of the type described above. Chemical growth of ZnO and TiO₂ structures with very large aspect ratios have been reported by various techniques.^[32–34] In addition, electrochemical deposition has successfully been employed in the literature to obtain conformal deposition of films into deeply-structured substrates.^[15] Doped metal oxide films are routinely fabricated by electrodeposition.^[35] A two-step (electro)chemical process is therefore proposed for the fabrication of high-aspect ratio metal oxide homojunction nanostructure arrays. Such a process is expected to accomplish fabrication at low temperatures, which suggests compatibility with low-cost and flexible substrates. Experiments of this type are currently underway in the authors' laboratories. Additional future work includes the in-depth analysis of the long-term stability of the dopants and their concentration profiles under operating conditions, a theoretical prediction of the optimal electrode three-dimensional geometry based on known material properties, as well as an analysis of optimal material systems suitable for this technique.

This report has introduced and experimentally verified the conceptual framework for the design of solar water oxidation photoelectrodes based on the spatially inhomogeneous doping of metal oxide nanostructures. Optical absorption and electronic conduction can be decoupled and optimized by spatially segregating the functional impurity species that facilitate their associated physical processes. The nanostructure regions possess functional specificity that is established by their chemical composition and three-dimensional geometry, which includes volume, orientation with respect to the direction of light propagation, as well as proximity to the semiconductor-liquid interface. Experimental results indicate optical absorption at visible wavelengths and the related water oxidation conversion efficiencies can be enhanced by physically distributing absorbing crystallites along the direction of light propagation while maintaining their close proximity to the oxide-water interface. An optimization pathway based on these results, analogous to the well-known optimization procedures for excitonic photovoltaic devices, has been suggested.

Experimental Section

The nanostructures were fabricated through a combination of electrochemical deposition and physical vapor deposition. Physical, optical, and photoelectrochemical characterization were performed by standard techniques. Experimental details are provided in the Supporting Information.

Supporting Information

Supporting Information is available from the Wiley Online Library or from the author.

Acknowledgements

This research was supported by Sandia National Laboratories. Sandia National Laboratories is a multi-program laboratory managed and operated by Sandia Corporation, a wholly owned subsidiary of Lockheed

Martin Corporation, for the U.S. Department of Energy's National Nuclear Security Administration under contract DE-AC04-94AL85000. The research has been partially supported by the U.S. Department of Energy, Office of Energy Efficiency and Renewable Energy.

Received: July 27, 2011

Revised: September 5, 2011

Published online: November 16, 2011

-
- [1] N. S. Lewis, D. G. Nocera, *Proc. Natl. Acad. Sci.* **2006**, *103*, 15729.
- [2] N. S. Lewis, *J. Electroanal. Chem.* **2001**, *508*, 1.
- [3] J. Augustynski, G. Calzaferri, J. C. Courvoisier, M. Grätzel, in *Proc. of the 11th World Hydrogen Energy Conference* (Eds: T. N. Veziroglu, C. J. Winter, J. P. Baselt, G. Kreysa), Stuttgart, **1996**, 2379.
- [4] E. L. Miller, R. E. Rocheleau, X. M. Deng, *Int. J. Hydrogen Energy* **2003**, *28*, 615.
- [5] M. G. Walter, E. L. Warren, J. R. McKone, S. W. Boettcher, Q. Mi, E. A. Santori, N. S. Lewis, *Chem. Rev.* **2010**, *110*, 6446.
- [6] B. D. Alexander, P. J. Kulesza, I. Rutkowska, R. Solarskac, J. Augustynski, *J. Mater. Chem.* **2008**, *18*, 2298.
- [7] *On Solar Hydrogen & Nanotechnology*, (Ed: L. Vayssieres), Wiley, Singapore **2009**.
- [8] M. A. Malati, W. K. Wong, *Surf. Technol.* **1984**, *22*, 305.
- [9] K. Rajeshwar, *J. Appl. Electrochem.* **2007**, *37*, 765.
- [10] Z. Zou, J. Ye, K. Sayama, H. Arakawa, *Nature* **2001**, *414*, 625.
- [11] B. A. Gregg, *J. Phys. Chem. B* **2003**, *107*, 4688.
- [12] M. Grätzel, *Inorg. Chem.* **2005**, *44*, 6841.
- [13] A. J. Nozik, *Nano Lett.* **2010**, *10*, 2735.
- [14] G. Wang, X. Yang, F. Qian, J. Z. Zhang, Y. Li, *Nano Lett.* **2010**, *10*, 1088.
- [15] K. Ernst, A. Belaidi, R. Könenkamp, *Semicond. Sci. Technol.* **2003**, *18*, 475.
- [16] J. Glasscock, P. R. F. Barnes, I. C. Plumb, A. Bendavid, P. J. Martin, in *Proc. of SPIE, the International Society for Optical Engineering* (Ed: L. Vayssieres), **2006**, 6340, 63400N.
- [17] K. Sivula, F. Le Formal, M. Grätzel, *Chem. Mater.* **2009**, *21*, 2862.
- [18] R. Könenkamp, K. Boedeker, M. C. Lux-Steiner, M. Poschenrieder, F. Zenia, C. Levy-Clement, S. Wagner, *Appl. Phys. Lett.* **2000**, *77*, 2575.
- [19] H. P. He, Tang, Z. Z. Ye, L. P. Zhu, B. H. Zhao, L. Wang, X. H. Li, *Appl. Phys. Lett.* **2007**, *90*, 023104.
- [20] D. Fichou, J. Pouliquen, J. Kossanyi, M. Jakani, G. Campet, J. Claverie, *J. Electroanal. Chem.* **1985**, *188*, 167.
- [21] H. A. Weakliem, *J. Chem. Phys.* **1962**, *36*, 2117.
- [22] X. Yang, A. Wolcott, G. Wang, A. Sob, R. C. Fitzmorris, F. Qian, J. Z. Zhang, Y. Li, *Nano Lett.* **2009**, *9*, 2331.
- [23] D. A. Schwartz, N. S. Norberg, Q. P. Nguyen, J. M. Parker, D. R. Gamelin, *J. Am. Chem. Soc.* **2003**, *125*, 13205.
- [24] W. K. Liu, G. Mackay Salley, D. R. Gamelin, *J. Phys. Chem. B* **2005**, *109*, 14486.
- [25] K. R. Kittilstved, W. K. Liu, D. R. Gamelin, *Nature Mater.* **2006**, *5*, 291.
- [26] C. A. Johnson, T. C. Kaspar, S. A. Chambers, G. Mackay Salley, D. R. Gamelin, *Phys. Rev. B* **1993**, *48*, 8672.
- [27] J. M. Noras, J. W. Allen, *J. Phys. C.: Solid State Phys.* **1980**, *13*, 3511.
- [28] A. J. Nozik, R. Memming, *J. Phys. Chem.* **1996**, *100*, 13061.
- [29] A. Mendoza-Galván, C. Trejo-Cruz, J. Lee, D. Bhattacharyya, J. Metson, P. J. Evans, U. Pal, *J. Appl. Phys.* **2006**, *99*, 014306.
- [30] M. D. Kelzenberg, S. W. Boettcher, J. A. Petykiewicz, D. B. Turner-Evans, M. C. Putnam, E. L. Warren, J. M. Spurgeon, R. M. Briggs, N. S. Lewis, H. A. Atwater, *Nature Mater.* **2010**, *9*, 239.
- [31] M. Grätzel, *Nature* **2001**, *414*, 338.
- [32] M. Law, L. E. Greene, J. C. Johnson, R. Saykally, P. Yang, *Nature Mater.* **2005**, *4*, 455.
- [33] X. Feng, K. Shankar, O. K. Varghese, M. Paulose, T. J. Latempa, C. A. Grimes, *Nano Lett.* **2008**, *8*, 3781.
- [34] G. K. Mor, K. Shankar, M. Paulose, O. K. Varghese, C. A. Grimes, *Nano Lett.* **2006**, *6*, 215.
- [35] T. F. Jaramillo, S.-H. Baeck, A. Kleiman-Shwarsstein, K.-S. Choi, G. D. Stucky, E. W. McFarland, *J. Comb. Chem.* **2005**, *7*, 264.
-